Applied Catalysis B: Environmental 160–161 (2014) 614–620

Contents lists available at ScienceDirect

Applied Catalysis B: Environmental

journal homepage: www.elsevier.com/locate/apcatb

Enhancement of photocatalytic H_2 evolution on $ZnIn_2S_4$ loaded with *in-situ* photo-deposited MoS_2 under visible light irradiation

Guoping Chen[a,b], Ning Ding[a,b], Fan Li[a,b], Yuzun Fan[c], Yanhong Luo[a,b], Dongmei Li[a,b,*], Qingbo Meng[a,b,*]

[a] Key Laboratory for Renewable Energy (CAS), Institute of Physics, Chinese Academy of Sciences, Beijing 100190, China
[b] Beijing Key Laboratory for New Energy Materials and Devices, Institute of Physics, Chinese Academy of Sciences, Beijing 100190, China
[c] Key Laboratory of Bio-Inspired Smart Interfacial Science and Technology of Ministry of Education, School of Chemistry and Environment, Beihang University, Beijing 100191, China

ARTICLE INFO

Article history:
Received 10 February 2014
Received in revised form 12 May 2014
Accepted 18 May 2014
Available online 27 May 2014

Keywords:
$ZnIn_2S_4$
In-situ photo-assisted deposition
H_2 evolution
MoS_2 co-catalyst
Photocatalysis

ABSTRACT

A new $MoS_2/ZnIn_2S_4$ photocatalyst system has been designed for H_2 evolution under visible light irradiation ($\lambda > 420$ nm), which was obtained by hydrothermal method to afford floriated $ZnIn_2S_4$ microspheres, and MoS_2 co-catalyst was subsequently loaded onto the $ZnIn_2S_4$ surface *via* a facile *in-situ* photo-assisted deposition process. The effects of hydrothermal temperature, the In/Zn molar ratios on the crystal structure, morphology, optical property as well as photocatalytic activity have been investigated in detail. Especially, the loading amount and deposition method of the MoS_2 co-catalyst are found to dramatically influence the photocatalytic activity of H_2 evolution. Up to 8.047 mmol h^{-1} g^{-1} of H_2 evolution rate has been achieved, 28 times higher than that of untreated $ZnIn_2S_4$. This work provides a new synthetic way to increase the photocatalytic activity of $MoS_2/ZnIn_2S_4$.

1. Introduction

Ever-increasing global energy demand and the ever-worsening environmental pollution associated with burning fossil fuels have stimulated people to explore clean and sustainable energy resources. As an ideal substitution of fossil fuels, hydrogen energy has been considered as an ideal future energy carrier, however, the traditional hydrogen production methods significantly restricted its widely application. Since Fujishima–Honda effect of water splitting using a TiO_2 electrode was reported in 1972 [1], the semiconductor-based photocatalysis has been an attractive and economic strategy to produce hydrogen energy [2–5]. To the photocatalytic water splitting process, developing highly efficient photocatalysts is undoubtedly the key. The specific requirements for photocatalytic materials generally include efficient light absorption, effective separation of the photo-generated charge carriers and efficient carrier transfer to the interface to directly release hydrogen and/or oxygen from water. Specially, the width of the band gap and the positions of conduction band (CB) and valence band (VB) of the semiconductor photocatalysts are the most important issues. Some wide band gap metal oxide photocatalysts with suitable band structures, such as TiO_2 [6,7], La-doped $NaTaO_3$ [8], $SrTiO_3$ [9], $K_4Nb_6O_{17}$ [10], *etc.*, exhibited good photocatalytic activity and stability, however, they are only active toward the UV light, which only accounts for ~4% of solar energy. Currently, exploring visible light-driven photocatalysts covering a wide solar spectrum, is of great desire in current research.

In contrast to metal oxides, metal sulfides possess relatively higher VB position, which is beneficial for band gap narrowing and expanding the light response to the visible light range. Besides, some metal sulfide photocatalysts have more negative CB position suitable for H_2O reduction [11]. Currently, some sulfide systems for H_2 evolution have been developed, such as Pt–PdS/CdS [12], NiS/CdS [13], MoS_2/CdS [14], ZnS–WS_2/CdS [15,16], $(AgIn)_xZn_{2(1-x)}S_2$ solid solutions [17] and so on.

As a member of the AB_2X_4 family semiconductors with a layered structure, ternary chalcogenide $ZnIn_2S_4$ is a good candidate for the photocatalysts under the visible light irradiation due to its suitable band gap (2.34–2.48 eV). Besides, it has other attractive advantages, such as low toxicity, considerable chemical stability and facile preparation process [21]. $ZnIn_2S_4$ photocatalyst for water splitting into H_2 was first reported by Li and Domen et al., and

* Corresponding authors at: Institute of Physics, CAS, Renewable Energy Lab, Zhongguancun South Third Street 8, Beijing, China. Tel.: +86 10 82649242; fax: +86 10 82649242.
E-mail addresses: dmli@iphy.ac.cn (D. Li), qbmeng@iphy.ac.cn (Q. Meng).

http://dx.doi.org/10.1016/j.apcatb.2014.05.028
0926-3373/

no deactivation was observed after 150 h photocatalytic reaction, indicating its excellent stability [22]. Since then, many efforts have been made to develop a variety of $ZnIn_2S_4$ photocatalysts with specific morphologies (*i.e.* nanotubes, nanoribbons, nanowires, and flower-like microspheres) as well as new preparative methods. For example, Guo et al. reported flowering-cherry-like $ZnIn_2S_4$ microspheres and micro-clusters *via* hydrothermal/solvothermal method, which gave a hydrogen evolution rate of 27.3 μmol h^{-1} [23–25]. Qian et al. employed hexagonal $ZnIn_2S_4$ photocatalyst with 3D-hierarchical persimmon-like shape for photosplitting water into H_2, which exhibited 220.45 μmol h^{-1} of H_2 evolution rate while simultaneous loading 3 wt% Pt co-catalyst. However, the photocatalytic activity of $ZnIn_2S_4$ itself was unsatisfactory [26]. Therefore, on the one hand, some doped $ZnIn_2S_4$ photocatalysts (*i.e.* Cu, Ni, Co and alkaline earth metals-doped) were developed in order to enhance the H_2 evolution activity [23,27–30]. On the other hand, $ZnIn_2S_4$-based composite photocatalysts have also been investigated, such as MWCNTs/$ZnIn_2S_4$ [31], CdS/$ZnIn_2S_4$ [32], $CuInS_2$/$ZnIn_2S_4$ [33], In_2S_3/$ZnIn_2S_4$ [34], NiS/$ZnIn_2S_4$ [35], MoS_2/$ZnIn_2S_4$ [36], RGO/$ZnIn_2S_4$ [37], $ZnIn_2S_4$/MnS (or CuS, CoS and so on) [38]. Typically, Pt loaded ZnS (17 mol%)-$ZnIn_2S_4$ photocatalyst exhibited 103 μmol of H_2 gas after 10 h irradiation with simultaneous degradation of glucose. However, up to now, the photocatalytic performance of $ZnIn_2S_4$-based photocatalysts is still unsatisfactory [39].

It is well known that co-catalysts are always indispensable for visible-light-driven metal sulfides photocatalysts to obtain high photocatalytic H_2 evolution activity. Noble metal Pt is the most common co-catalyst to $ZnIn_2S_4$ photocatalyst systems, whereas inexpensive non-Pt cocatalyst materials have been rarely used. Recently, MoS_2 and WS_2 were reported as efficient co-catalyst replacement for Pt in CdS or $ZnIn_2S_4$ photocatalytic systems [15,36,40–43]. Herein, we demonstrate an efficient MoS_2/$ZnIn_2S_4$ photocatalyst system for H_2 evolution under visible light irradiation. Floriated $ZnIn_2S_4$ microspheres were synthesized by a simple hydrothermal method, on which was subsequently loaded by MoS_2 co-catalyst *via* a facile *in-situ* photo-assisted deposition process [44]. Up to 8.047 mmol h^{-1} g^{-1} of H_2 evolution rate has been achieved by loading MoS_2 as a co-catalyst, higher than those of Pt/$ZnIn_2S_4$ and known MoS_2/$ZnIn_2S_4$ under the same reaction condition.

2. Experimental

2.1. Reagents and chemicals

Zinc chloride ($ZnCl_2$), indium chloride tetrahydrate ($InCl_3{\cdot}4H_2O$), thioacetamide (CH_3CSNH_2), hydrochloric acid (HCl), lactic acid ($C_3H_6O_3$) and ethanol (CH_3CH_2OH) were analytical reagents and used as received. $(NH_4)_2MoS_4$ was synthesized according to the literature method [45].

2.2. Syntheses of $ZnIn_2S_4$ microspheres and MoS_2/$ZnIn_2S_4$ samples

Hexagonal $ZnIn_2S_4$ microspheres were synthesized by hydrothermal method according to Refs. [36,46], except for the temperature range 200–250 °C. The $ZnIn_2S_4$ samples obtained at different hydrothermal temperatures were labeled as ZIS-*x* (*x* means the hydrothermal temperature) and the $ZnIn_2S_4$ samples with different molar ratios of In/Zn were labeled as ZIS-*x*-*y* (*y* means the molar ratio of In/Zn).

A typical *in-situ* synthetic process of MoS_2/$ZnIn_2S_4$ samples is given in Section 2.4, since it is directly used for the photocatalytic performance. Samples with different amount of MoS_2 (0.125–1.0 wt%) were prepared by using different amount of $(NH_4)_2MoS_4$ while keeping other conditions the same.

For comparison, MoS_2/$ZnIn_2S_4$ samples were also prepared by our ball-milling combined calcination method [15,40]. That is, the mixture of a proper amount of $(NH_4)_2MoS_4$ and 1 g $ZnIn_2S_4$ powder was ball-milled at the speed of 450 r min^{-1} for 4 h, then the ball-milled powder was calcined at 673 K for 2 h in Ar atmosphere to afford the MoS_2/$ZnIn_2S_4$ sample.

2.3. Characterization

The surface morphologies of the samples were characterized by a scanning electron microscope (SEM, XL30 S-FEG, FEI) and a transmission electron microscope (TEM, FEI Tecnai F20 Super-twin). X-ray diffraction (XRD) patterns were collected by a rotating-anode diffractometer with Cu K_α radiation (M18X-AHF, MacScience). Each sample was scanned through in a 2θ range of 10–80°. X-ray photoelectron spectra (XPS) were recorded on an ULVAC-PHI X-ray photoelectron spectrometer (PHI Quantera SXM) using Al K_α radiation. All binding energies were referred to the C1s peak of 284.8 eV. UV–vis diffuse reflection of the samples was determined on Hitachi U-4100 UV–vis-near-IR spectrophotometer. Nitrogen adsorption–desorption isotherms were collected on ASAP2020 apparatus, Micromeritics. The thermal decomposition behavior of the MoS_2/$ZnIn_2S_4$ sample was studied by a differential thermal analysis/thermogravimetric analysis instrument (DTA/TGA, NETZSCH STA 449C) in N_2 atmosphere with a heating rate of 10 K min^{-1} in a temperature range 300–1073 K.

2.4. Photocatalytic performance

The photocatalytic reactions were carried out in a Pyrex reaction cell connected to a closed gas circulation and evacuation system. 0.1 g as-prepared $ZnIn_2S_4$ powder or a proper amount of $(NH_4)_2MoS_4$ were dispersed by sonication for 2 min in a 150 mL aqueous solution containing 15 mL lactic acid as the sacrificial reagent. Then the suspension was thoroughly degassed and irradiated by 300 W Xe lamp (PLS-SXE300, Trusttech) equipped with an optical filter ($\lambda > 420$ nm) to cut off ultraviolet light and a water filter to remove infrared light. The temperature of the reaction solution was maintained at 293 ± 1.5 K by a flow of cooling liquid. The evolved H_2 amount was determined by an on-line gas chromatography with a thermal conductivity detector (SP6890, molecular sieve 5 Å column, Ar carrier). The photocatalytic activities were compared by the average H_2 evolution rate in the first 5 h.

3. Results and discussion

3.1. XRD analyses

The samples labeled as ZIS-*x* (*x* = 200–250), which were derived from different hydrothermal temperatures (*x* = 200, 210, 220, 230, 240, 250) while fixing the reactant molar ratio of In/Zn at 1:1.5, can present the similar XRD patterns, as shown in Fig. 1. They are hexagonal $ZnIn_2S_4$ (JCPDS: 65-2023) with good phase purity, in agreement with the previous work [19,35,36,46–48]. Besides, with increasing the hydrothermal temperature, the crystallinity of $ZnIn_2S_4$ improves.

Furthermore, the $ZnIn_2S_4$ samples with different molar ratios of In/Zn (ZIS-250-*y*, *y* = 1.0–2.0) were also investigated. As shown in Fig. 2, the diffraction patterns of all the samples are different with each other. When the reactant molar ratio of In/Zn is 1:1 (ZIS-250-1), the diffraction patterns are ascribed to the combination of hexagonal $ZnIn_2S_4$ (JCPDS: 65-2023) and hexagonal ZnS (JCPDS: 36-1450). Obviously, the ZIS-250-1 is impure mainly due to excessive $ZnCl_2$ in the reaction. With the increase of the molar ratios

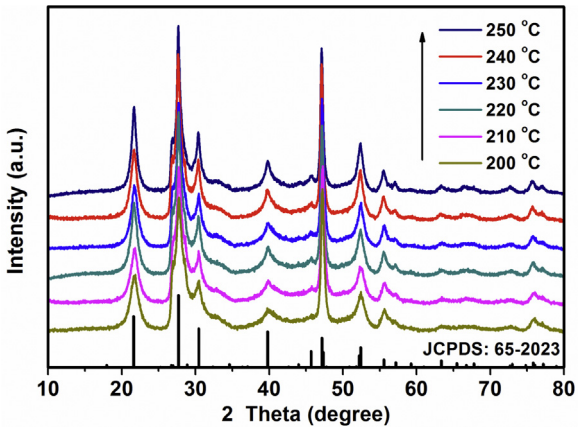

Fig. 1. XRD patterns of ZIS-*x* samples prepared at hydrothermal temperatures ranging from 200 to 250 °C for 6 h with the In/Zn molar ratio fixed at 1.5.

of In/Zn, the purity of $ZnIn_2S_4$ will be improved. When the molar ratio of In/Zn is 1:1.5, pure hexagonal $ZnIn_2S_4$ is obtained. However, when the molar ratio of In/Zn is higher than 1:1.75, some impurity peaks marked with black dots appear in Fig. 2, which is supposed to be a small amount of $In_{0.14}Zn_{0.33}S_{0.53}$ (JCPDS: 24-1451).

3.2. Microstructure analyses

Fig. 3a–f shows the SEM images of the ZIS-*x* (x = 200–250) series samples. As can be seen, after hydrothermal treatment, the $ZnIn_2S_4$ crystallites self-assemble into floriated microspheres, and each microsphere is comprised of numerous petals formed zigzag structure, resulting in macropores or mesopores between petals, in agreement with the literature results [23,49]. It has been proved that the $ZnIn_2S_4$ microspheres are self-assembled from small crystal nucleuses, which may be related to the layered feature of hexagonal $ZnIn_2S_4$ [50]. With the enhancement of the hydrothermal temperatures, the diameters of $ZnIn_2S_4$ microspheres enlarge gradually. When the hydrothermal temperature is 200 °C, the average diameter of the $ZnIn_2S_4$ microspheres is relatively small, ranging from 2 to 4 μm, except for a small quantity of ultra large ones. The ZIS-210 microspheres are generally larger ranging from 4 to 7 μm. Instead, the ZIS-250 microspheres show relatively uniform particle size distribution which average diameters are ranging from 5 to 8 μm. To the ZIS-250-*y* series samples, typical microsphere morphologies are also observed as the ZIS-*x* series without obvious difference.

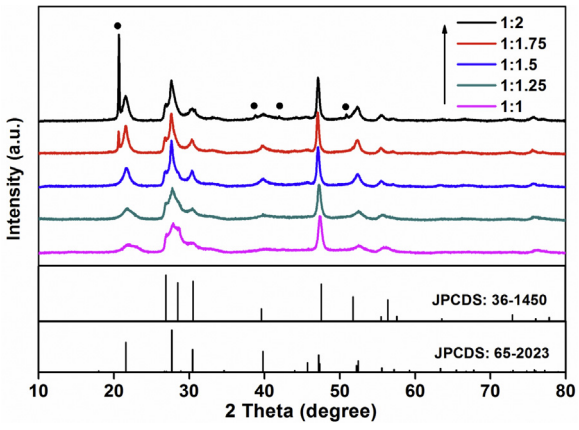

Fig. 2. XRD patterns of ZIS-250-*y* with different molar ratios of In/Zn (1.0–2.0) based on ZIS-250 samples, the symbol "•" represents the impurity.

Further investigation about the structure of the $ZnIn_2S_4$ microsphere was carried out by TEM and HRTEM. Fig. 4a clearly shows that the petals with various orientations forming zigzag structure, which is in accordance with the SEM images in Fig. 3. The HRTEM image of the petals is shown in Fig. 4b, which interplaner spacing are 0.32 and 0.33 nm, in agreement with (1 0 2) and (1 0 0) planes of hexagonal $ZnIn_2S_4$, respectively.

3.3. UV–vis diffuse reflectance absorption spectra

Fig. 5 shows the UV–vis diffuse reflectance absorption spectra of the ZIS-250-*y* series samples. As shown in Fig. 5, an obvious red-shift of the absorption edges is observed with the enhancement of the molar ratios of In/Zn from 1:1 to 1:2 for ZIS-250-*y* series, suggesting that the band gap of $ZnIn_2S_4$ gradually decreases. Similar phenomena are also observed in $Zn_xCd_{1-x}S$ (x = 0 to 1) series photocatalysts [20,51,52]. The band gap values are given in the inset of Fig. 5, which are estimated from the intersection of the extrapolated linear potion in a related curve of $(\alpha h\upsilon)^{1/2}$ *vs.* photon energy, that is, the band gap values of the ZIS-250-*y* series are 2.58, 2.56, 2.55, 2.49, and 2.44 eV, respectively, corresponding to the molar ratios of In/Zn in a range from 1 to 2.

3.4. In-situ photodeposition of MoS_2 on $ZnIn_2S_4$

As an efficient non-Pt co-catalyst, MoS_2 has been proved to improve the photocatalytic activity of CdS photocatalytic systems. In this work, new $MoS_2/ZnIn_2S_4$ photocatalytic systems have been prepared. In order to realize the homogeneous deposition of MoS_2 on the surface of $ZnIn_2S_4$ photocatalysts, the ball-milling combined calcination method developed in our lab was first attempted [15,40]. A detailed process is as follows: a proper amount of $(NH_4)_2MoS_4$ was mixed with 1 g of $ZnIn_2S_4$ and 2 mL of ethanol in an agate jar, which was ball-milled for 4 h at the speed of 450 r min^{-1}. Finally, the ball-milled powder was calcined at 400 °C in Ar atmosphere for 2 h to afford $MoS_2/ZnIn_2S_4$ sample. The sample color changed from bright yellow to black. In comparison with untreated $ZnIn_2S_4$, the morphology of $MoS_2/ZnIn_2S_4$ sample changes a lot, that is, $ZnIn_2S_4$ microspheres completely collapse, as shown in Fig. 3g. Further DTA/TGA investigation in Ar atmosphere revealed that calcination does not bring the thermal decomposition of $MoS_2/ZnIn_2S_4$-250 in the temperature range 300–1073 K. Accordingly, thermal treatment will cause significant change of the $ZnIn_2S_4$ morphology as well as the photocatalytic activity (see Section 3.5). Obviously, this ball-milling combined calcination method is not suitable for $MoS_2/ZnIn_2S_4$ samples.

Here, the photo-assisted deposition method is adopted to load MoS_2 co-catalyst on $ZnIn_2S_4$ with a little modification, which mechanism is similar to that of photo-assisted deposition of Pt using H_2PtCl_6 as the precursor [44]. As can be seen in Fig. 3h, the morphology of $MoS_2/ZnIn_2S_4$ sample does not change in comparison with those of $ZnIn_2S_4$ samples, that is, the photo-assisted deposition of MoS_2 cannot bring the change in the morphology of $ZnIn_2S_4$ microspheres. In fact, the distribution and size of MoS_2 on $ZnIn_2S_4$ microspheres in the ZIS-*x*-*y* series cannot be observed by SEM because the amount of MoS_2 on the surface of $ZnIn_2S_4$ is too low. In order to further verify the existence of MoS_2 and chemical valence state of Mo atom in the composite photocatalyst, 3 wt% $MoS_2/ZnIn_2S_4$ photocatalyst was characterized by XPS spectra. As shown in Fig. 6, only Zn, In, S, and Mo elements were detected except for C and O. The peaks at 444.1 and 451.7 eV correspond to the binding energies of $In3d_{5/2}$ and $In3d_{3/2}$ of $ZnIn_2S_4$, respectively. The peaks at 1021.0 and 1044.0 eV correspond to the binding energies of $Zn2p_{3/2}$ and $Zn2p_{1/2}$ of $ZnIn_2S_4$, respectively. The broad asymmetric curve of S2p can be deconvoluted into two peaks with binding energies of 161.96 and 162.89 eV, corresponding

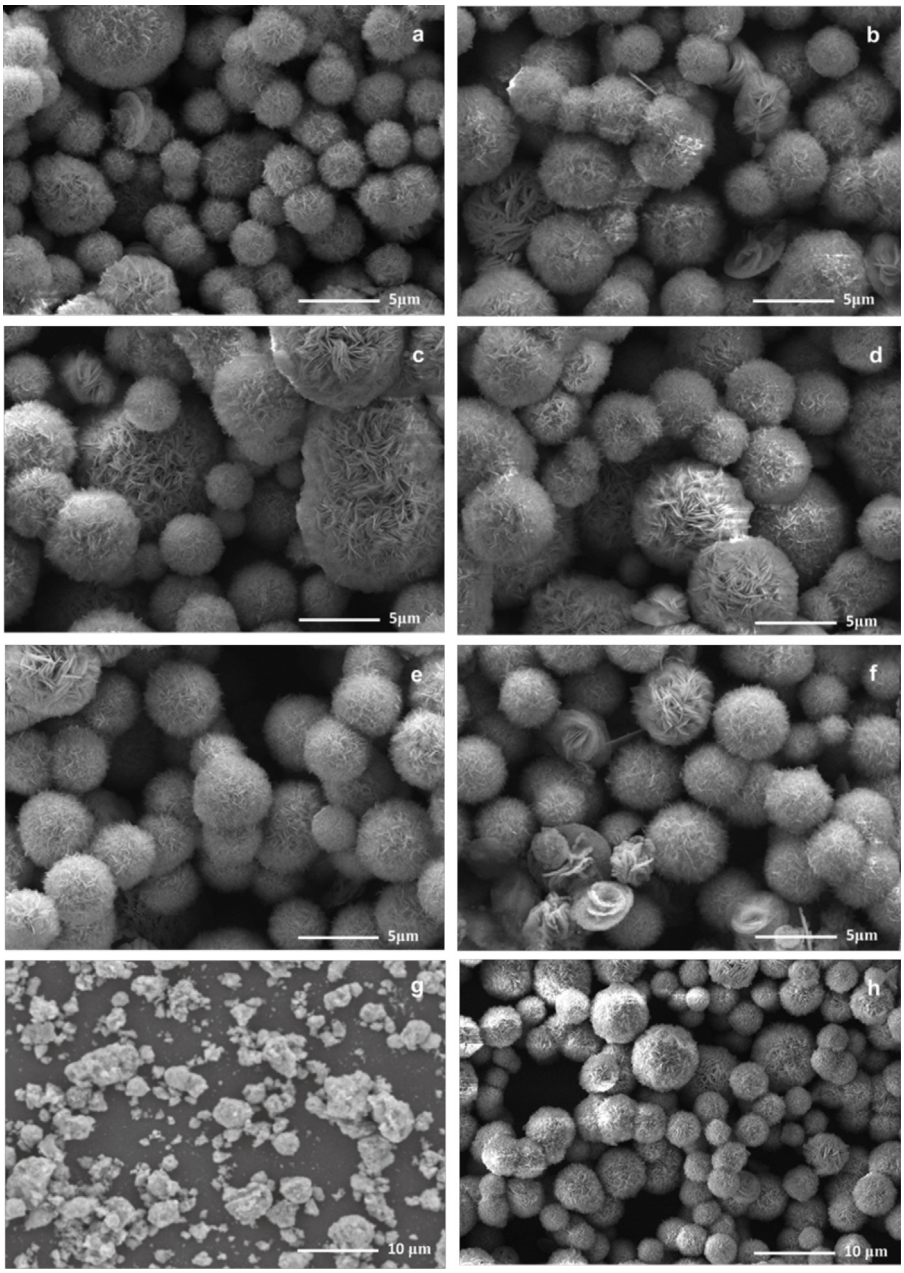

Fig. 3. SEM images of ZIS-*x* (*x* = 200–250) samples at different hydrothermal temperatures with the molar ratio of In/Zn fixed at 1:1.5: (a) 200 °C; (b) 210 °C; (c) 220 °C; (d) 230 °C; (e) 240 °C; (f) 250 °C; (g) $MoS_2/ZnIn_2S_4$ sample derived from ball-milling combined calcination method; (h) 0.375 wt% $MoS_2/ZnIn_2S_4$ derived from *in-situ* photo-assisted deposition method.

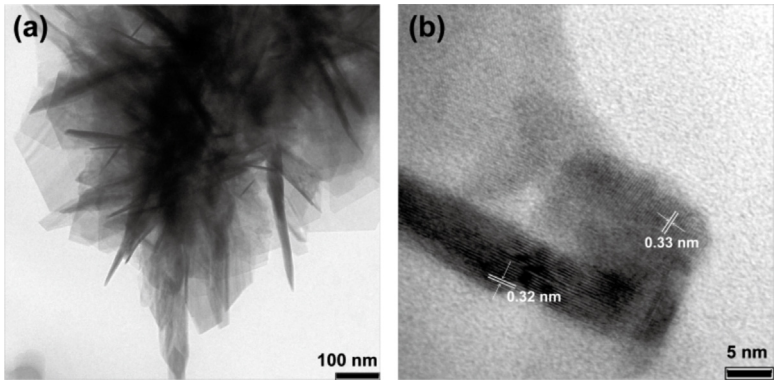

Fig. 4. TEM images of ZIS-250 samples with the In/Zn molar ratio of 1:1.5: (a) low magnification; (b) high magnification.

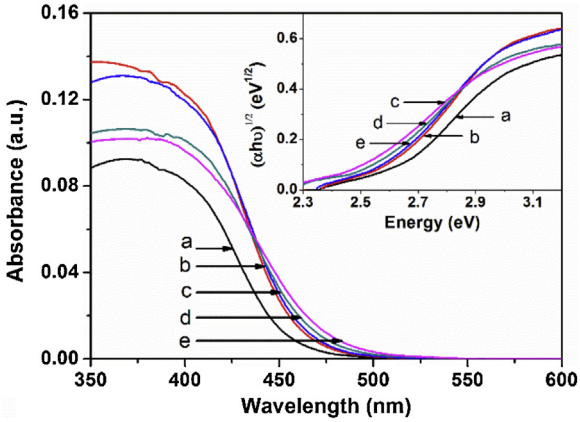

Fig. 5. UV–vis diffuse reflectance absorption spectra of the ZIS-250-*y* series products: (a) $y = 1$; (b) $y = 1.25$; (c) $y = 1.5$; (d) $y = 1.75$; (e) $y = 2$. Inset: the relationship between $(\alpha h\upsilon)^{1/2}$ and photon energy. (For interpretation of the references to color in this figure legend, the reader is referred to the web version of this article.)

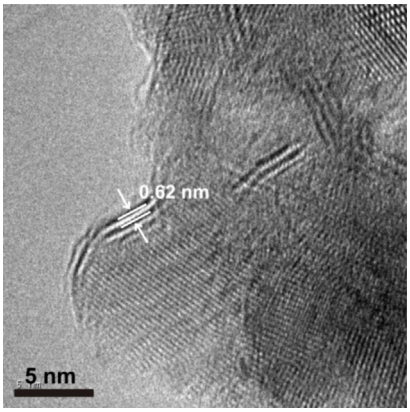

Fig. 7. HRTEM image of 3 wt% MoS_2/ZIS-250 photocatalyst.

to $S2p_{3/2}$ and $S2p_{1/2}$ of $ZnIn_2S_4$, respectively [35]. The peaks at 228.7 and 231.9 eV correspond to the binding energy of $Mo3d_{5/2}$ and $Mo3d_{3/2}$, respectively, indicating the formation of MoS_2 from $(NH_4)_2MoS_4$ precursor [40,42].

Further investigation on the junction structure between MoS_2 and $ZnIn_2S_4$ of 3 wt% $MoS_2/ZnIn_2S_4$ photocatalyst was carried out by HRTEM. As shown in Fig. 7, co-catalyst MoS_2 with typical layered structure is dispersed on the $ZnIn_2S_4$ surface. The interplaner spacing is 0.62 nm, corresponding to the (0 0 2) plane of hexagonal MoS_2. The good interfacial contact between MoS_2 and $ZnIn_2S_4$ favors the electron transfer from $ZnIn_2S_4$ to MoS_2 [40,42].

The color of the $MoS_2/ZnIn_2S_4$ photocatalysts changes from bright yellow to yellow–green after *in-situ* photodeposition MoS_2 on the surface of $ZnIn_2S_4$. Fig. 8 shows the UV–vis diffuse reflectance absorption spectra of the MoS_2/ZIS-250 photocatalysts with different MoS_2 loading amounts. As can be seen, no obvious absorption edge shift of $ZnIn_2S_4$ is observed, but the absorption intensity gradually enhances with the increase of the loading amount of MoS_2, indicating that MoS_2 is indeed loaded on the surface of $ZnIn_2S_4$.

3.5. Investigation of photocatalytic H_2 evolution activities

Fig. 9a shows the H_2 evolution rates of MoS_2/ZIS-250 photocatalysts with different loading amount of MoS_2. $ZnIn_2S_4$ alone exhibits a very low photocatalytic activity with the H_2 evolution rate of 0.283 mmol h^{-1} g^{-1}, indicating that $ZnIn_2S_4$ lacks catalytic sites for H_2 reduction reaction. In the meantime, when MoS_2 alone is used as the photocatalyst, no H_2 is detected, suggesting MoS_2 itself is inactive to photocatalytic hydrogen evolution, in good agreement with the literatures [15,36,53]. However, when 0.125 wt% of MoS_2 is loaded on the $ZnIn_2S_4$ surface, the H_2 evolution rate significantly enhances to 4.054 mmol h^{-1} g^{-1}. With increasing the MoS_2 loading amount, the H_2 evolution rate is further enhanced, reaching the maximum value 8.047 mmol h^{-1} g^{-1} for 0.375 wt% $MoS_2/ZnIn_2S_4$. However, further increase the loading amount of MoS_2 on $ZnIn_2S_4$ surface will lead to a decrease in the photocatalytic H_2 evolution. Such a decrease in the photocatalytic activity with a heavy loading of MoS_2 may be derived from the shading effect of MoS_2, which can block the light absorption of $ZnIn_2S_4$ [15,36]. For comparison, Pt co-catalyst is also loaded on

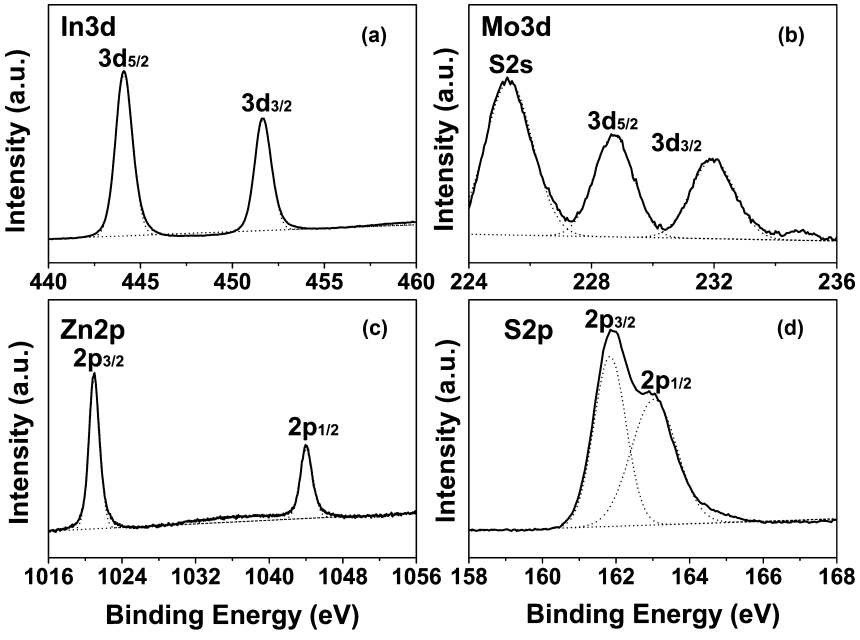

Fig. 6. XPS spectra of 3 wt% $MoS_2/ZnIn_2S_4$ photocatalyst: (a) In3d core-level spectra; (b) Mo3d core-level spectra; (c) Zn2p core-level spectra; (d) S2p core-level spectra.

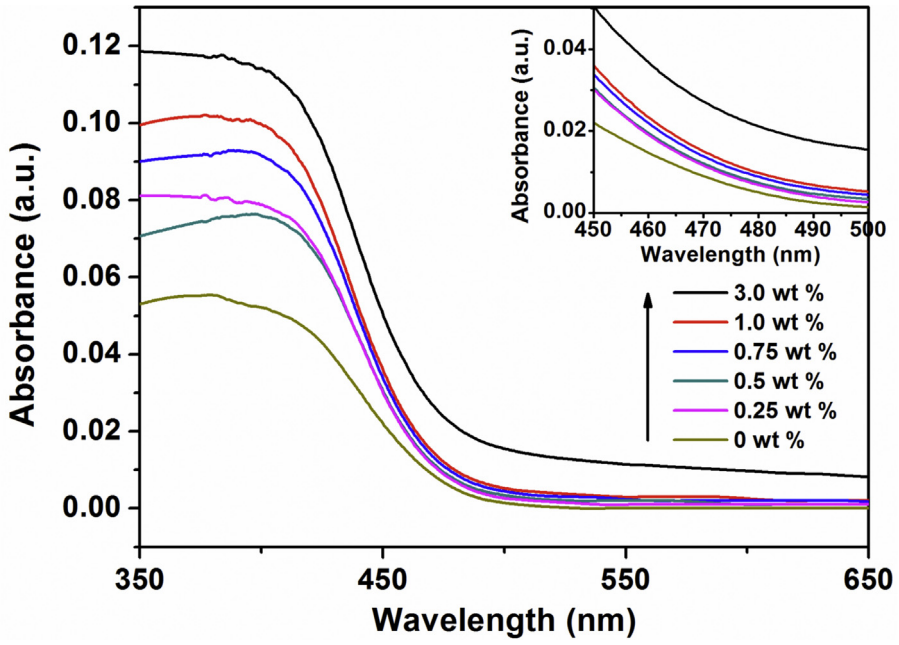

Fig. 8. Diffuse reflectance absorption spectra of the MoS_2/ZIS-250 photocatalysts with different MoS_2 loading amounts. Inset: the enlarged diffuse reflectance absorption spectra in the range 450 to 500 nm. (For interpretation of the references to color in this figure legend, the reader is referred to the web version of this article.)

the $ZnIn_2S_4$ surface by *in-situ* photo-deposition method. Optimal Pt deposition amount is 0.2 wt% for Pt-$ZnIn_2S_4$ samples, which can present the H_2 evolution rate of 5.117 mmol h^{-1} g^{-1}, indicating MoS_2 can exhibit much better catalytic activity than conventional Pt co-catalyst to $ZnIn_2S_4$ systems [22,24].

In terms of 0.375 wt% MoS_2/ZIS-*x* photocatalyst, the effect of different hydrothermal temperatures on the H_2 evolution rates was also investigated, as shown in Fig. 9b. As can be seen, with increasing hydrothermal temperatures, the H_2 evolution rate gradually increases, which are 4.443, 4.871, 5.833, 5.895, 6.331 and 8.047 mmol h^{-1} g^{-1} for ZIS-200, ZIS-210, ZIS-220, ZIS-230, ZIS-240 and ZIS-250, respectively. There are several possible factors accounted for the improved photocatalytic H_2 evolution rates, such as the crystallinity and specific surface areas. The surface areas increase from 41.76 to 58.35 m^2 g^{-1} for the samples ZIS-200–250, which can provide more catalytic sites for the photocatalytic reaction. In the meantime, the crystallinity of the $ZnIn_2S_4$ samples is getting improved as the hydrothermal temperature increasing. As a consequence, it is suggested that the defects of the samples themselves and the recombination of photogenerated electron and hole pairs in the photocatalytic process are well suppressed, leading to the improvement of photocatalytic activity as well.

Fig. 10 shows the effect of the photocatalyst composition with different In/Zn molar ratios on the H_2 evolution rate. With the increase of the In/Zn molar ratio, the photocataytic H_2 evolution rate increases first, then decreases gradually. As shown in the UV–vis absorbance spectra, the UV–vis absorption edges of the samples are red-shifted with the In/Zn increased from 1 to 1.5, indicating the enhanced visible light absorption. In the meantime, the XRD results also suggest that the purity of the samples is getting improved with the In/Zn molar ratio changing from 1 to 1.5. Therefore, the photocataytic H_2 evolution rate increases firstly. However, when the In/Zn molar ratio exceeds 1.5, other impurity phase forms (such as $In_{0.14}Zn_{0.33}S_{0.53}$), which may be recombination centers of photogenerated electron and hole pairs in the photocatalytic process, thus resulting in the gradual decrease of the photocataytic H_2 evolution rate.

In terms of our previous work and the literatures, it is suggested that the photoexcited electrons transfer from $ZnIn_2S_4$ to MoS_2, where H^+ is reduced to hydrogen atom, then releases H_2, while

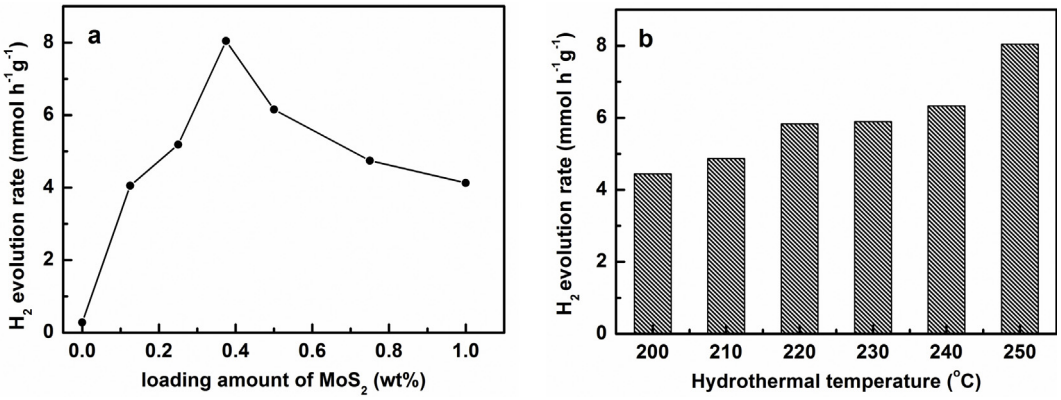

Fig. 9. (a) H_2 evolution rates on the MoS_2/ZIS-250 photocatalytic systems with different amounts of MoS_2 co-catalysts; (b) H_2 evolution rates on 0.375 wt% MoS_2/ZIS-*x* photocatalysts with different hydrothermal temperatures. Photocatalytic reaction conditions: 0.1 g catalyst; 150 mL solution containing 15 mL lactic acid as sacrificial reagent; light source, xenon lamp (300 W) with a cutoff filter ($\lambda > 420$ nm) as the light source.

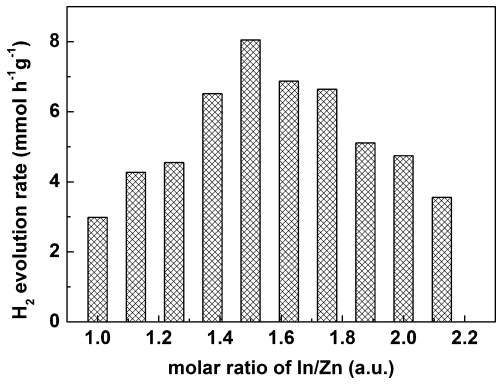

Fig. 10. H_2 evolution rate of 0.375 wt% MoS_2/ZIS-250-*y* photocatalysts with different In/Zn molar ratios under visible light irradiation ($\lambda > 420$ nm). Photocatalytic reaction conditions: 0.1 g catalyst; 150 mL solution containing 15 mL lactic acid as sacrificial reagent; light source, xenon lamp (300 W) with a cutoff filter ($\lambda > 420$ nm) as the light source.

the holes oxidize the sacrificial agents [40,43]. The existence MoS_2 on the $ZnIn_2S_4$ surface can effectively restrain the reaction between the holes and $ZnIn_2S_4$, thus facilitating the photocatalytic reaction.

4. Conclusions

A new $MoS_2/ZnIn_2S_4$ photocatalyst system has been designed for H_2 evolution under visible light irradiation ($\lambda > 420$ nm). The $ZnIn_2S_4$ photocatalysts were synthesized *via* a simple hydrothermal method, and a facile *in-situ* photo-assisted deposition method was subsequently employed to realize the MoS_2 cocatalyst loaded onto the $ZnIn_2S_4$ surface. All the products exhibit similar floriated microsphere morphologies. It has been revealed that the hydrothermal temperature and the reactant molar ratio of In/Zn have significant effects on crystal structures, optical properties, and photocatalytic activities of $MoS_2/ZnIn_2S_4$ photocatalysts. Up to 8.047 mmol h^{-1} g^{-1} of H_2 evolution rate has been achieved, which is based on 0.375 wt% $MoS_2/ZnIn_2S_4$ photocatalyst, higher than those of un-treated $ZnIn_2S_4$ and conventional $Pt/ZnIn_2S_4$ and $MoS_2/ZnIn_2S_4$ photocatalysts. Therefore, MoS_2 as a cost-effective cocatalytst for the $ZnIn_2S_4$ photocatalyst exhibits potential application in the photocatalytic H_2 evolution.

Acknowledgments

The work was financially supported by the National Natural Science Foundation of China (nos. 21173260, 51072221 and 91233202), the Ministry of Science and Technology of the People's Republic of China (973 Project, nos. 2012CB932903 and 2012CB932904) and the Knowledge Innovation Program of the Chinese Academy of Sciences.

References

[1] A. Fujishima, K. Honda, Nature 238 (1972) 37–38.
[2] M. Yosuki, T. Takata, K. Domen, Coord. Chem. Rev. 257 (2013) 1957–1969.
[3] R. Abe, J. Photochem. Photobiol., C: Photochem. Rev. 11 (2010) 179–209.
[4] K. Maeda, K. Domen, J. Phys. Chem. Lett. 1 (2010) 2655–2661.
[5] A. Kudo, Y. Miseki, Chem. Soc. Rev. 38 (2009) 253–278.
[6] S. Tabata, H. Nishida, Y. Masaki, K. Tabata, Catal. Lett. 34 (1995) 245–249.
[7] K. Sayama, H. Arakawa, J. Chem. Soc., Faraday Trans. 93 (1997) 1647–1654.
[8] H. Kato, K. Asakura, A. Kudo, J. Am. Chem. Soc. 125 (2003) 3082–3089.
[9] J.J. Zou, C.J. Liu, Acta Phys. Chim. Sin. 22 (2006) 926–931.
[10] K. Domen, A. Kudo, M. Shibata, A. Tanaka, K. Maruya, T. Onishi, J. Chem. Soc., Chem. Commun. 23 (1986) 1706–1707.
[11] K. Zhang, L.J. Guo, Catal. Sci. Technol. 3 (2013) 1672–1690.
[12] J.H. Yang, H.J. Yan, X.L. Wang, F.Y. Wen, Z.J. Wang, D.Y. Fan, J.Y. Shi, C. Li, J. Catal. 290 (2012) 151–157.
[13] W. Zhang, Y. Wang, Z. Wang, Z. Zhong, R. Xu, Chem. Commun. 46 (2010) 7631–7633.
[14] X. Zong, G.P. Wu, H.J. Yan, G.J. Ma, J.Y. Shi, F.Y. Wen, L. Wang, C. Li, J. Phys. Chem. C 114 (2010) 1963–1968.
[15] G. Chen, F. Li, Y. Fan, Y. Luo, D. Li, Q. Meng, Catal. Commun. 40 (2013) 51–54.
[16] F.Z. Jia, Z.P. Yao, Z.H. Jiang, Int. J. Hydrogen Energy 37 (2012) 3048–3055.
[17] I. Tsuji, H. Kato, H. Kobayashi, A. Kudo, J. Am. Chem. Soc. 126 (2004) 13406–13413.
[19] C.L. Li, J.A. Yuan, B.Y. Han, W.F. Shangguan, Int. J. Hydrogen Energy 36 (2011) 4271–4279.
[20] Y. Wang, J. Wu, J. Zheng, R. Xu, Catal. Sci. Technol. 1 (2011) 940–947.
[21] K. Zhang, L. Guo, Catal. Sci. Technol. 3 (2013) 1672–1690.
[22] Z. Lei, W. You, M. Liu, G. Zhou, T. Takata, M. Hara, K. Domen, C. Li, Chem. Commun. 39 (2003) 2142–2143.
[23] S.H. Shen, L. Zhao, Z.H. Zhou, L.J. Guo, J. Phys. Chem. C 112 (2008) 16148–16155.
[24] S.H. Shen, L. Zhao, L.J. Guo, Int. J. Hydrogen Energy 33 (2008) 4501–4510.
[25] S.H. Shen, L. Zhao, L.J. Guo, Mater. Res. Bull. 44 (2009) 100–105.
[26] J. Shen, J.T. Zai, Y.P. Yuan, X.F. Qian, Int. J. Hydrogen Energy 37 (2012) 16986–16993.
[27] D. Jing, M. Liu, L. Guo, Catal. Lett. 140 (2010) 167–171.
[28] W.H. Yuan, X.C. Liu, L. Li, Acta Phys. Chim. Sin. 29 (2013) 151–156.
[29] S.H. Shen, J. Chen, X.X. Wang, L. Zhao, L.J. Guo, J. Power Sources 196 (2011) 10112–10119.
[30] F. Li, G. Chen, J. Luo, Q. Huang, Y. Luo, Q. Meng, D. Li, Catal. Sci. Technol. 3 (2013) 1993–1999.
[31] B. Chai, T.Y. Peng, P. Zeng, X.H. Zhang, Dalton Trans. 41 (2012) 1179–1186.
[32] Y. Yu, G. Chen, G. Wang, Z. Lv, Int. J. Hydrogen Energy 38 (2012) 1278–1285.
[33] V.V. Bozhko, A.V. Novosad, G.E. Davidyuk, V.R. Kozer, O.V. Parasyuk, N. Vainorius, V. Janonis, A. Sakavicius, V. Kazukauskas, J. Alloys Compd. 553 (2013) 48–52.
[34] Z.W. Mei, S.X. Ouyang, D.M. Tang, T. Kako, D. Golberg, J.H. Ye, Dalton Trans. 42 (2013) 2687–2690.
[35] L. Wei, Y. Chen, J. Zhao, Z. Li, Beilstein J. Nanotechnol. 4 (2013) 949–955.
[36] L. Wei, Y. Chen, Y. Lin, H. Wu, R. Yuan, Z. Li, Appl. Catal., B: Environ. 144 (2014) 521–527.
[37] J. Zhou, G.H. Tian, Y.J. Chen, X.Y. Meng, Y.H. Shi, X.R. Cao, K. Pan, H.G. Fu, Chem. Commun. 49 (2013) 2237–2239.
[38] S. Shen, X. Chen, F. Ren, C.X. Kronawitter, S.S. Mao, L.J. Guo, Nanoscale Res. Lett. 6 (2011) 290.
[39] Y.X. Li, J.X. Wang, S.Q. Peng, G.X. Lu, S.B. Li, Int. J. Hydrogen Energy 35 (2010) 7116–7126.
[40] G.P. Chen, D.M. Li, F. Li, Y.Z. Fan, H.F. Zhao, Y.H. Luo, R.C. Yu, Q.B. Meng, Appl. Catal., A: Gen. 443 (2012) 138–144.
[41] X. Zong, Y. Na, F. Wen, G. Ma, J. Yang, D. Wang, Y. Ma, M. Wang, L. Sun, C. Li, Chem. Commun. 45 (2009) 4536–4538.
[42] X. Zong, H. Yan, G. Wu, G. Ma, F. Wen, L. Wang, C. Li, J. Am. Chem. Soc. 130 (2008) 7176–7177.
[43] X. Zong, J.F. Han, G.J. Ma, H.J. Yan, G.P. Wu, C. Li, J. Phys. Chem. C 115 (2011) 12202–12208.
[44] M. Nguyen, P.D. Tran, S.S. Pramana, R.L. Lee, S.K. Batabyal, N. Mathews, L.H. Wong, M. Grätzel, Nanoscale 5 (2013) 1479–1482.
[45] W.H. Pan, M.E. Leonowicz, E.I. Stiefel, Inorg. Chem. 22 (1983) 672–678.
[46] Y. Chen, R. Huang, D. Chen, Y. Wang, W. Liu, X. Li, Z. Li, ACS Appl. Mater. Interfaces 4 (2012) 2273–2279.
[47] B. Chai, T.Y. Peng, P. Zeng, X.H. Zhang, X.J. Liu, J. Phys. Chem. C 115 (2011) 6149–6155.
[48] Y.J. Chen, S.W. Hu, W.J. Liu, X.Y. Chen, L. Wu, X.X. Wang, P. Liu, Z.H. Li, Dalton Trans. 40 (2011) 2607–2613.
[49] S.H. Shen, L. Zhao, L.J. Guo, J. Phys. Chem. Solids 69 (2008) 2426–2432.
[50] Z.X. Chen, D.Z. Li, W.J. Zhang, C. Chen, W.J. Li, M. Sun, Y.H. He, X.Z. Fu, Inorg. Chem. 47 (2008) 9766–9772.
[51] K. Zhang, D.W. Jing, C.J. Xing, L.J. Guo, Int. J. Hydrogen Energy 32 (2007) 4685–4691.
[52] C.J. Xing, Y.J. Zhang, W. Yan, L.J. Guo, Int. J. Hydrogen Energy 31 (2006) 2018–2024.
[53] G. Tian, Y. Chen, Z. Ren, C. Tian, K. Pan, W. Zhou, J. Wang, H. Fu, Chem. Asian J. 9 (2014) 1291–1297.